Improved Seasonal Drought Forecasts using Reference Evapotranspiration Anomalies

Daniel J. McEvoy[1, 2], Justin L. Huntington[1, 2], John F. Mejia[1], and Michael T. Hobbins[3, 4]

[1]Desert Research Institute, Reno, Nevada, USA

[2]Western Regional Climate Center, Reno, Nevada, USA

[3]Cooperative Institute for Research in Environmental Sciences, Boulder, Colorado, USA

[4]NOAA Earth System Research Laboratory, Physical Sciences Division, Boulder, Colorado, USA

Key Points:

- Seasonal forecasts of ET_0 often have higher skill than do precipitation forecasts.
- Greatest ET_0 forecast skill is found in agricultural regions of the U.S. during the growing season.
- Major improvements are found when forecasts are initialized during moderate and strong ENSO.

Corresponding Author:

Daniel J. McEvoy

Desert Research Institute-Western Regional Climate Center

2215 Raggio Parkway

Reno, Nevada, 89512

E-mail: mcevoyd@dri.edu

Abstract

A novel CONUS-wide evaluation of reference evapotranspiration (ET_0; a formulation of evaporative demand) anomalies is performed using the Climate Forecast System version 2 (CFSv2) reforecast data for 1982-2009. This evaluation was motivated by recent research showing ET_0 anomalies can accurately represent drought through exploitation of the complementary relationship between actual evapotranspiration and ET_0. Moderate forecast skill of ET_0 was found up to leads of five months, and was consistently better than precipitation skill over most of CONUS. Forecasts of ET_0 during drought events revealed high categorical skill during notable warm-season droughts of 1988 and 1999 in the central and northeast CONUS, and the winter/spring drought of 1992 in the northwest. Increased ET_0 skill was found in several climate regions when CFSv2 forecasts were initialized during moderate-to-strong El Niño-Southern Oscillation events. Our findings suggest that ET_0 anomaly forecasts can improve and complement existing seasonal drought forecasts.

1. Introduction

A growing literature indicates that current dynamical seasonal precipitation (*Prcp*) forecasts contain limited skill past a one-month lead time [e.g., *Lavers et al.,* 2009; *Yuan et al.,* 2011; *Yuan et al.,* 2013*; Saha et al.,* 2014; *Wood et al.*, 2015]. Therefore, incorporating new drought-related variables with higher skill could add value and confidence to operational seasonal drought forecasts. Our understanding of drought dynamics and variability has evolved substantially over the last decade as evapotranspiration (*ET*) and physically based evaporative demand [reference *ET* (ET_0); *Allen et al.,* 2005] has been shown to couple the land surface and atmosphere and so can be used in drought indicators [e.g., *Yao et al.,* 2010; *Anderson et al.,* 2011; *Mu et al.,* 2013; *Otkin et al.,* 2013; *Shukla et al.,* 2015; *McEvoy*, 2015]. Anomalously high ET_0 is one of the contributing factors to intensification of extreme drought events, such as the 2012-present California drought [*Shukla et al.,* 2015; *Williams et al.,* 2015].

Research on seasonal ET_0 forecasts are limited to *Tian et al.* [2014], who evaluated bias-corrected maximum and minimum temperature (T_{max} and T_{min}, respectively), wind speed (U_z), downwelling shortwave radiation (R_d), and ET_0 over the southeast CONUS. *Tian et al.* [2014] found Climate Forecast System version 2 [CFSv2; *Saha et al.,* 2014] ET_0 forecasts to have moderate skill during the cold season with the greatest skill when forecasts were initialized during El Niño-Southern Oscillation (ENSO) events (El Niño or La Niña conditions existed), and no skill during the warm season due to the inability of CFSv2 to fully resolve summer convection. An extensive CONUS wide skill analysis of CFSv2 ET_0, its drivers, and seasonal drought forecasting is absent from the literature, and is the focus of this letter.

As an example of *Prcp* and ET_0 anomalies during drought, Figure 1 illustrates ET_0 (Figure 1a) and *Prcp* (Figure 1b) anomaly percentiles (with respect to a base period of 1982-

2009) using gridded METDATA [*Abatzoglou,* 2011], for AMJ of 2002 period, one of the most severe droughts in the recorded history of the Southwest [e.g., *Weiss et al.,* 2009 and references therein]. Both ET_0 and *Prcp* anomalies identify similar magnitude and spatial patterns of wet (northwest MT and the Great Lakes) and dry regions (the Southwest and the mid-Atlantic coast), and clearly demonstrate that ET_0 can successfully identify drought patterns (further comparison presented in Figure S1). This occurs through (1) regional atmospheric dynamics that increase surface irradiance (through decreased cloudiness) and the vapor pressure deficit (through increased air temperature (T_{air}) and decreased humidity) and (2) local land surface-atmosphere feedbacks that lead to a complementary relationship between ET_0 and actual *ET* (a proxy for *Prcp*) under water limitations [*Hobbins and Huntington*, 2015; *McEvoy*, 2015]. In this letter, anomalies in ET_0 are derived from CFSv2 reforecasts (CFSRF) are evaluated over CONUS against METDATA in order to determine (1) if forecasts of ET_0 anomalies and its driving variables are skillful and in what regions, and (2) if ET_0 anomalies can be forecast with greater skill than *Prcp* anomalies during droughts.

2. Data and Methodology

Nine-month continuous reforecasts from CFSv2 were obtained from NCEP, covering the retrospective period of 1982-2009. A detailed description of CFSRF can be found in *Saha et al.* [2014], and several other papers have presented CFSRF data distribution format [e.g., *Yuan et al.,* 2011; *Dirmeyer,* 2013]. Monthly ensembles (mean of forecasts initialized within the same month and year only) were created from CFSRF leads of 1-9 months, resulting in a range of 20 to 28 ensemble members per month (Table S1). This allows us to identify the impact of initialization month on forecast skill. To evaluate CFSRF skill we use METDATA [*Abatzoglou,* 2011] for 1982-2009. METDATA is a bias-corrected and spatially disaggregated (from 12 km to

93 4 km) product that combines the Parameter Regression on Independent Slopes Model [PRISM;
94 *Daly et al.,* 1994] with the North American Land Data Assimilation System version 2 [NLDAS-
95 2; *Mitchell et al.*, 2004). To test the sensitivity of observations to forecast skill, two other gridded
96 data sets were also considered—the Climate Forecast System Reanalysis and the Modern Era
97 Retrospective-analysis for Research and Applications—but differences in results as compared to
98 using METDATA were negligible (not shown). To match the CFSRF spatial resolution,
99 METDATA was averaged from daily to monthly values and resampled from 4 km to 1° using a
100 bilinear interpolation. The following monthly variables were evaluated at 1° spatial resolution:
101 *Prcp*, T_{max} (at 2 m), T_{min} (at 2 m), q (at 2 m), U_z (at 10 m), and R_d.
102 Following recommendations of *Allen et al.* [2005; equation 1], ET_0 was computed with
103 the American Society of Civil Engineers Standardized Penman-Monteith equation using monthly
104 METDATA and CFSRF. A priori, it is generally assumed that if the necessary data are available,
105 ET_0 should be used over a T_{air}- and or radiation-based method [*Hobbins et al*., 2008; *Allen et al.*,
106 2005]. *Hobbins* [2015] demonstrated that the dominant drivers of ET_0 vary across CONUS
107 depending on factors such as aggregation period (monthly vs. annual) and season, and T_{air} is not
108 always the dominant driver.
109 The CONUS wide skill analysis of ET_0 and its drivers was carried out and summarized
110 over area-averaging domains using the nine National Climatic Data Center (NCDC) climate
111 regions (Figure 1c; *Karl and Koss,* 1984). Monthly and seasonal METDATA ET_0 anomalies
112 were computed relative to the 1982-2009 monthly and seasonal climatology. Following the
113 recommendation of *Kumar et al.* [2014], monthly CFSRF ET_0 anomalies were calculated relative
114 to the CFSRF monthly climatology (1982-2009) from the corresponding initialization month and
115 lead time. Season-one forecasts are defined as the accumulated anomaly over the first three

116 months after the initialization month (e.g., season-one JFM forecasts are initialized in December,
117 and represent the accumulated anomaly over JFM).

118 To assess skill of CFSRF, temporal anomaly correlations [AC; *Miyakoda et al.,* 1972;
119 equation 11] between CFSRF ensemble mean ET_0 and METDATA ET_0 were computed at
120 monthly 1-9 month leads, and the season-one forecasts (skill of ET_0 drivers is provided in
121 supplemental material). ACs were computed for each grid point through time and then spatially
122 averaged over each climate region. Skill during individual drought events was assessed based on
123 the probability forecasts using the categorical Heidke skill score [HSS; *O'Lenic et al.,* 2008,
124 *Peng et al.,* 2013] (see supplemental material for details). Drought events were defined based on
125 METDATA when seasonal anomalies indicated at least 50% of the regional area is above the
126 80th percentile for ET_0 and below the 20th percentile for *Prcp* (though not necessarily identical
127 grid points). This excludes events where ET_0 and *Prcp* show contrasting drought signals.
128 Percentile thresholds were chosen based on the U.S. Drought Monitor classification scheme for
129 moderate drought. For each drought event a spatial HSS was calculated using all grid points for
130 each climate region.

131 **3. Results**

132 **3.1 Deterministic skill**

133 Figure 2 shows spatially averaged monthly AC for ET_0 (Figure 2f-2j and 2p-2t) and *Prcp*
134 (Figure 2a-2e and 2k-2o) over CONUS and its constituent NCDC climate regions. The National
135 Oceanic and Atmospheric Administration's (NOAA) CPC currently uses an AC value of 0.3 as
136 the threshold for a skill mask (AC < 0.3 being considered to have no skill) in the real time
137 CFSv2 forecasts. Maximum ET_0 AC for each region ranged from 0.41 (Southeast; Figure 2t) to
138 0.66 (West; Figure 2q). Moderate skill (AC = 0.3 to 0.6) in ET_0 was maintained for important

late winter and early growing season months of January through May for the Southwest, South, and West at one to five month lead times (Figure 2r, 2s, and 2q, respectively), and for important late growing season and harvest period months of July through September for the East North Central, Central, and Northeast at one to three months (Figure 2h, 2i, and 2j, respectively). For these same regions, months, and lead time ranges, consistent *Prcp* skill was absent. The West, Southwest, and South regions all show a similar pattern of a sharp decline in ET_0 skill for target months of July through December. For *Prcp* skill a similar yet less congruent and weaker skill pattern is evident over the West and Southwest regions, where enhanced *Prcp* predictability stems from initial conditions of ENSO region sea surface temperatures (SSTs) [e.g., *Wood et al.*, 2005; *Yuan et al.,* 2013]. This suggests that ET_0 predictability in these regions may also be related to SST initial conditions from the ENSO region in the late-summer and fall months, a hypothesis we examine further in subsequent sections.

In decomposing ET_0 drivers of T_{max}, T_{min}, R_d, and q, it was found that ET_0 skill is mostly a result of skill in T_{max} (Figure S2), T_{min} (Figure S3), and q (Figure S4). For some regions, such as the Southwest, ET_0 and q actually have greater skill than T_{max} and T_{min} at times, which supports the conclusion that T_{air} is not always the dominant driver of ET_0 variability [*Hobbins*, 2015]. In regions and months when R_d (Southeast region) and U_z (Soutwest and West regions) are the dominant drivers of ET_0 variability [*Hobbins*, 2015], poor skill in monthly forecasts of R_d and U_z (Figures S5 and S6 for, respectively) is likely adding to degraded overall ET_0 skill.

A more seasonal focused comparison of ET_0 and *Prcp* skill is provided below that highlights pertinent information on where and when ET_0 can add value to seasonal drought forecasts. Figure 3 illustrates season-one AC for both ET_0 and *Prcp* averaged over CONUS and the nine US climate regions. CONUS-wide, ET_0 skill is greater than *Prcp* during all seasons, and

remains above the 0.3 AC moderate skill threshold for more than half of the year. Most regions contain at least one or two seasons when ET_0 skill is much greater than *Prcp* (AC differences [$AC_{ET0} - AC_{Prcp}$] of ~0.2 to 0.5). Of particular interest are regions where ET_0 skill is high compared to *Prcp* skill during the growing season, such as in the East North Central, Central, and Northeast regions, where enhanced reliability in seasonal drought forecasts could greatly benefit agricultural operations during mid and late season crop harvest periods. A second area of interest is in the Southwest region, where moderate ET_0 skill during the fall, winter, and spring can result in improved water supply outlooks.

3.2 Categorical skill of probability forecasts during drought events

Figure 4 illustrates region specific scatter plots of season-one ET_0 HSS (x-axis) and *Prcp* HSS (y-axis) during drought events. Overall, two regions (Southwest and East North Central) were found to have positive (skillful) mean HSS using ET_0, while no regions were found to have positive mean HSS using *Prcp*. Although the mean HSS across all season-one ET_0 forecasts was not skillful for most regions, many notable drought events were forecast skillfully with ET_0 and not with *Prcp*, as seen in the lower right ET_0 only skill quadrant of Figure 4 (quadrants defined by black reference lines) where there are more than double the number of events than the upper left *Prcp* only skill quadrant (38 and 15 total events in all regions for the lower right and upper left quadrants, respectively). Drought events, such as the summer (JJA) of 1988, one of the worst droughts in the Central US since the infamous "dust bowl", were forecast well using both ET_0 and Prcp in the West North Central and East North Central regions. However, positive skill was only found with ET_0 in the Central region. Another event that was forecast well with ET_0 and where *Prcp* skill was poor was the summer and fall of 1999, a drought event that had devastating impacts on the Central and Northeast regions. The aforementioned drought events are annotated

185 in Figure 4.These results illustrate that ET_0 forecasts generally have higher skill than *Prcp*
186 forecasts for predicting drought events.

187 **3.3 ENSO as a source of predictability**

188 Seasonal forecast skill of T_{air} and *Prcp* over CONUS, and ET_0 over a portion of the
189 Southeast region, have been found to increase when CFSRF and global spectral model
190 (predecessor to CFS) forecasts are initialized during moderate and strong ENSO events [*Wood et*
191 *al.,* 2005; *Yuan et al.,* 2013; *Tian et al.,* 2014]. To investigate ENSO as a source of ET_0
192 predictability over CONUS, all season-one forecasts were compared against ENSO conditional
193 forecasts defined as when the Oceanic Nino Index (ONI) from the CPC
194 (http://www.cpc.ncep.noaa.gov/products/analysis_monitoring/ensostuff/ensoyears.shtml)
195 exceeds +/- 1° C. ONI is one of several ENSO indices and results could vary depending on
196 choice of index [e.g., *Capotondi et al.,* 2015]. Only forecasts initialized during ENSO events
197 were considered, not the month for which the forecast was made. A total of 76 ENSO conditional
198 initialization months were classified during the period of record out of 336 possible season-one
199 forecasts, and 52 out of 76 ENSO initial months occurred in fall-winter (September through
200 February). Results are only shown for fall-winter; the seasons when ENSO has the greatest
201 impacts on CONUS. Temporal AC was computed over each grid point for fall-winter ENSO
202 conditional and all fall-winter season-one forecasts, and then spatially averaged over each
203 climate region. A caveat to this approach is that forecasts may not be completely independent of
204 each other (e.g., a forecast made in November for DJF and one made in December for JFM rely
205 on independent atmospheric initial conditions but ENSO region SSTs may be similar) which
206 may reduce the degrees of freedom in a given sample.

Figure 5 shows the difference in AC between fall-winter ENSO conditional initial months and all fall-winter forecasts using ET_0 (Figure 5a) and *Prcp* (Figure 5b). Spatial patterns of forecast improvement (positive AC differences) are quite similar for both ET_0 and *Prcp* over parts of the West, Southwest, South and Southeast regions. Improvements in forecast skill of *Prcp* are consistent with previous research in the West, Southeast, and Southwest regions [e.g., *Wood et al.,* 2005; *Yuan et al.,* 2013] and are consistent with *Tian et al.* [2014] over the Southeast region for ET_0. Spatial patters of ET_0 and *Prcp* AC difference are contrasting in much of the northern half of CONUS, where ET_0 forecasts are greatly improved in the Northwest region, while *Prcp* forecasts are improved in the Northeast and Central regions. Overall, ET_0 skill is considerably higher than *Prcp* during ENSO conditional forecasts (Figure 5c and 5d). This is particularly evident in the Northwest and Southwest regions, with similar skill found in the West and Southeast regions, and only minor changes in skill were found in the South, West North Central, and East North Central regions.

4. Discussion and Conclusions

This study highlights a novel CONUS-wide assessment of seasonal ET_0 forecast anomalies using CFSv2 reforecast (CFSRF) and METDATA observations. Nine climate regions were used as area-averaging domains to assess regional skill variability. Monthly ensemble mean forecasts were analyzed at leads of one to nine months, and season-one ensemble mean forecasts were used to highlight seasonal skill variability. Monthly ET_0 ACs revealed large regional and seasonal variability, with moderate skill (AC of 0.3-0.6) found at leads of one to five months and no consistent skill at longer lead times.

Seasonal ET_0 skill was found to be consistently greater than *Prcp* skill when averaged over CONUS, and the same is true for most regions where large AC differences (0.2-0.5) were

found depending on season. Assessment of probability forecasts during drought events using the HSS revealed high skill in ET_0 for some regions and seasons, particularly over the Southwest and East North Central regions. Three of the most severe droughts during the period of record (summer of 1988, fall of 1999, and winter and spring of 1992) were all forecast with reasonable skill using ET_0 and with poor skill using *Prcp*. While it is still unclear what makes certain drought events more predictable than others, one prominent feature during 1988, 1992, and 1999 (Northeast only) was high T_{air}, which likely improved ET_0 over *Prcp* forecasts. Another interesting finding is that poor *Prcp* forecasts are not always coincident with poor ET_0 forecasts, which potentially indicates a lack of land surface-atmospheric coupling in CFSv2 for certain drought events. Findings from ET_0 and *Prcp* skill analyses indicate that including ET_0 anomalies in operational seasonal drought forecasts would provide additional skill and confidence for various applications such as agricultural and water resource outlooks throughout CONUS.

Results illustrating the skill of ENSO conditional vs. all events show that some portion of ET_0 predictability comes from the initial state of tropical Pacific SSTs. This is evident from similar skill patterns found between ET_0 and *Prcp* in the West, Southwest, and Southeast regions (Figures 2 and 5), where several studies have found enhanced *Prcp* and T_{air} skill during strong ENSO events [e.g., *Wood et al.,* 2005; *Yuan et al.,* 2013]. *Tian et al.* [2014] also found enhanced ET_0 predictability in the Southeast during the cold season when CFSv2 forecasts were initialized during ENSO events. *Jia et al.* [2015] found seasonal *Prcp* skill from the Geophysical Fluid Dynamics Laboratory climate model to be mostly ENSO-related, but T_{air} skill to be related to ENSO in addition to a multi-decadal warming signal, which could be an additional factor contributing to ET_0 skill from CFSv2. *Peng et al.* [2013] also found that the warming trend in CFSv2 enhanced categorical T_{air} forecast skill (when compared to CFSv1) due to the addition of

253 a time-evolving carbon dioxide concentration not used in CFSv1. Initial state of the soil moisture
254 column could also be contributing to ET_0 predictability considering energy balance feedbacks
255 between the land and near surface boundary layer, thus affecting variables of T_{max}, T_{min}, and q
256 used to generate ET_0 estimates. *Yoon and Leung* [2015] found antecedent soil moisture to be as
257 important as ENSO in seasonal *Prcp* forecast skill over parts of CONUS, and given the high
258 correspondence in ET_0 and *Prcp* anomalies (Figures 1 and S1), it is expected that soil moisture
259 would be another source of predictability for ET_0 forecasts.

260 Skillful seasonal climate predictions remain a major challenge in drought forecasting,
261 however the use of ET_0 anomalies from CFSv2 clearly show improvements over *Prcp* forecasts
262 over most regions and seasons and can improve and complement existing seasonal drought
263 forecasts. Further research and skill improvements are needed for reliable operational use of ET_0
264 (and other metrics) in seasonal drought forecasting. Identifying why certain droughts are more
265 predictable than others is a research area that would greatly benefit operational seasonal drought
266 forecasting.

267

268 **Acknowledgments**

269 Daniel McEvoy, John Mejia, and Justin Huntington were all partially supported by the Desert
270 Research Institute (DRI) IBM PureSystems, Institute Project Assignments-Enhanced Seasonal
271 Forecasts for Western United States, Bureau of Reclamation Climate Analysis Tools
272 WaterSMART program (Public Law 111-11, Section 9504(b), Agreement # R11AP81454), and
273 the National Integrated Drought Information System (NIDIS). Michael Hobbins acknowledges
274 support from Inter-Agency Agreement AID-FFP-P-10-00002/006 between USAID and NOAA

for support to the Famine Early Warning Systems Network. Links to METDATA and CFSRF used in this study can be found in the references.

References

Abatzoglou, J. T. (2011), Development of gridded surface meteorological data for ecological applications and modeling. *Int. J. Climatol*. **33**, 121–131, DOI: 10.1002/joc.3413. [Data available at: http://nimbus.cos.uidaho.edu/DATA/OBS/.]

Allen, R.G., I.A. Walter, R. Elliott, T. Howell, D. Itenfisu, and M. Jensen (2005), The ASCE standardized reference evapotranspiration equation. Report 0-7844-0805-X, 59 pp. [Available online at: http://www.kimberly.uidaho.edu/water/asceewri/ascestzdetmain2005.pdf.]

Anderson, M. C., C. R. Hain, B. Wardlow, J. R. Mecikalski, and W. P. Kustas (2011), Evaluation of a drought index based on thermal remote sensing of evapotranspiration over the continental United States. *J. Climate*, **24**, 2025–2044, doi: 10.1175/2010JCLI3812.1.

Capotondi, A., A. T. Wittenberg, M. Newman, E. D. Lorenzo, J. Yu, P. Braconnot, J. Cole, B. Dewitte, B. Giese, E. Guilyardi, F. Jin, K. Karnauskas, B. Kirtman, T. Lee, N. Schneider, Y. Xue, and S. Yeh (2015), Understanding ENSO Diversity. *Bull. Amer. Meteor. Soc*., **96**, 921-938. doi: http://dx.doi.org/10.1175/BAMS-D-13-00117.1.

Daly, C., R. P. Neilson, and D. L. Phillips (1994), A statistical-topographic model for mapping climatological precipitation over mountainous terrain. *J. Appl. Meteor.,* **33,** 140-158.

Dirmeyer, P. A. (2013), Characteristics of the water cycle and land-atmosphere interactions from a comprehensive reforecast and reanalysis, Clim. Dyn., 41, 1083-1097, doi: 10.1007/s00382-013-1866-x.

297 Hobbins, M. T., A. Dai, M. L. Roderick, and G. D. Farquhar (2008), Revisiting the
298 parameterization of potential evaporation as a driver of long-term water balance
299 trends, *Geophys. Res. Lett*., **35**, L12403, doi: 10.1029/2008GL033840.
300 Hobbins, M. T., A. Wood, D. Streubel, and K. Werner (2012), What drives the variability of
301 evaporative demand across the conterminous United States? *J. Hydrometeor*, **13**, 1195–1214,
302 doi: 10.1175/JHM-D-11-0101.1.
303 Hobbins, M.T. (2015), The variability of ASCE Standardized Reference Evapotranspiration: a
304 rigorous, CONUS-wide decomposition and attribution. *Transactions of the ASABE* (in press).
305 Hobbins, M. T. and J. L. Huntington (2015), Chapter 44, in Handbook of applied hydrology,
306 edited by V. P. Singh, McGraw-Hill Education, New York, in press.
307 Jia, L., X. Yang, G. A. Vecchi, R. G. Gudgel, T. L. Delworth, A. Rosati, W. F. Stern, A. T.
308 Wittenberg, L. Krishnamurthy, S. Zhang, R. Msadek, S. Kapnick, S. Underwood, F. Zeng,
309 W. G. Anderson, V. Balaji, and Keith Dixon (2015), Improved Seasonal Prediction of
310 Temperature and Precipitation over Land in a High-Resolution GFDL Climate Model. *J.*
311 *Climate*, **28**, 2044–2062. doi: http://dx.doi.org/10.1175/JCLI-D-14-00112.1.
312 Karl T. R. and W. J. Koss (1984): Regional and national monthly, seasonal, and annual
313 temperature weighted by area, 1895-1983. *Historical Climatology Series 4-3*, National
314 Climatic Data Center, Asheville, NC, 38 pp.
315 Kumar, S., P. A. Dirmeyer, and J. L. Kinter III (2014), Usefulness of ensemble forecasts
316 from NCEP Climate Forecast System in sub-seasonal to intra-annual forecasting, *Geophys.*
317 *Res. Lett*., **41**, 3586–3593, doi:10.1002/2014GL059586.
318 Lavers, D., L. Luo, and E. F. Wood (2009), A multiple model assessment of seasonal climate
319 forecast skill for applications, *Geophys. Res. Lett*., **36**, L23711, doi:10.1029/2009GL041365.

McEvoy, D. J. (2015), Physically based evaporative demand as a drought metric: Historical analysis and seasonal prediction, Ph.D. dissertation, Dep. of Atmospheric Science, Univ. of Nevada, Reno, Nevada, USA. [Available online at: http://www.dri.edu/images/stories/divisions/das/dasfaculty/mcevoy_dissertation_final.pdf]

Mitchell, K. E. and coauthors (2004), The multi-institution North American Land Data Assimilation System (NLDAS): Utilizing multiple GCIP products and partners in a continental distributed hydrological modeling system, *J. Geophys. Res.*, 109, D07S90, doi:10.1029/2003JD003823.

Miyakoda, K., G. D., Hembree, R. F. Strickler, and I. Shulman (1972), Cumulative results of extended forecast experiments I. Model performance for winter cases. *Mon. Wea. Rev.***100**. 836-855, doi: 10.1175/1520-0493(1972)100<0836:CROEFE>2.3.CO;2.

Mu, Q., M. Zhao, J. S. Kimball, N. G. McDowell, S. W. Running (2013), A remotely sensed global terrestrial drought severity index. *Bull. Amer. Meteor. Soc.*, **94**, 93-98, doi: 10.1175/BAMS-D-11-00213.1.

O'lenic, E. A., D. A. Unger, M. S. Halpert, and K. S. Pelman (2008), Developments in operational long-range climate prediction at CPC. *Wea. Forecasting*, **23**, 496-515, doi: 10.1175/2007WAF2007042.1.

Otkin, J. A., M. C. Anderson, C. Hain, I. E. Mladenova, J. B. Basara, M. Svoboda (2013), Examining Rapid Onset Drought Development Using the Thermal Infrared–Based Evaporative Stress Index. *J. Hydrometeor.*, **14**, 1057–1074, doi: 10.1175/JHM-D-12-0144.1.

Peng, P., A. G. Barnston, and A. Kumar (2013), A comparison of skill between two versions of the NCEP Climate Forecast System (CFS) and CPC's operational short-lead seasonal outlooks. *Wea. Forecasting*, **28**, 445-462, doi: 10.1175/WAF-D-12-00057.1.

343 Saha S., and coauthors (2014), The NCEP Climate Forecast System Version 2. *J. Climate*, 27,
344 2185-2208. doi: http://dx.doi.org/10.1175/JCLI-D-12-00823.1. [Reforecast data available at:
345 http://nomads.ncdc.noaa.gov/data/cfsr-rfl-mmts/].
346 Shukla, S., M. Safeeq, A. AghaKouchak, K. Guan, and C. Funk (2015), Temperature impacts on
347 the water year 2014 drought in California. *Geophys. Res. Lett*., **42**,
348 doi:10.1002/2015GL063666.
349 Tian, D., C. J. Martinez, and W. D. Graham (2014), Seasonal prediction of regional reference
350 evapotranspiration based on Climate Forecast System Version 2. *J. Hydrometeor.*, **15**, 1166-
351 1188. doi: 10.1175/JHM-D-13-087.1.
352 Yao, Y., S. Liang, Q. Qin, K. Wang (2010), Monitoring Drought over the Conterminous United
353 States Using MODIS and NCEP Reanalysis-2 Data. *J. Appl. Meteor. Climatol*., **49**, 1665–
354 1680. doi: 10.1175/2010JAMC2328.1.
355 Yoon, J., and L. R. Leung (2015), Assessing the relative influence of surface soil moisture and
356 ENSO SST on precipitation predictability over the contiguous United States. *Geophys. Res.*
357 *Lett.*, doi: 10.1002/2015GL064139.
358 Yuan, X., E. F. Wood, L. Luo, and M. Pan (2011), A first look at Climate Forecast System
359 version 2 (CFSv2) for hydrological seasonal prediction. *Geophys. Res. Lett*., **38**, doi:
360 10.1029/2011GL047792.
361 Yuan, X., E. F. Wood, J. K. Roundy, and M. Pan (2013), CFSv2-based seasonal hydroclimatic
362 forecasts over the conterminous United States. *J. Hydrometeor*, **26**, 4828-4847,
363 doi: http://dx.doi.org/10.1175/JCLI-D-12-00683.1.

364 Weiss, J. L., C. L. Castro, and J. T. Overpeck (2009), Distinguishing pronounced droughts in the
365 Southwestern United States: seasonality and effects of warmer temperature. *J. Climate*, **22**,
366 5918-5932. doi: http://dx.doi.org/10.1175/2009JCLI2905.1.
367 Williams, A. P., R. Seager, J. T. Abatzoglou, B. I. Cook, J. E. Smerdon, and E. R. Cook, (2015),
368 Contribution of anthropogenic warming to California drought during 2012-2014. *Geophys.*
369 *Res. Lett*., doi: 10.1002/2015GL064924.
370 Wood, A. W., A. Kumar, and D. P. Lettenmaier (2005), A retrospective assessment of National
371 Centers for Environmental Prediction climate model–based ensemble hydrologic forecasting
372 in the western United States. *J. Geophys. Res*., **110**, D04105, doi: 10.1029/2004JD004508.
373
374 Wood, E., S. Schubert, A. Wood, C. Peters-Lidard, K. Mo, A. Mariotti, and R. Pulwarty (2015),
375 Prospects for advancing drought understanding, monitoring and prediction. *J. Hydrometeor*.
376 doi:10.1175/JHM-D-14-0164.1.
377

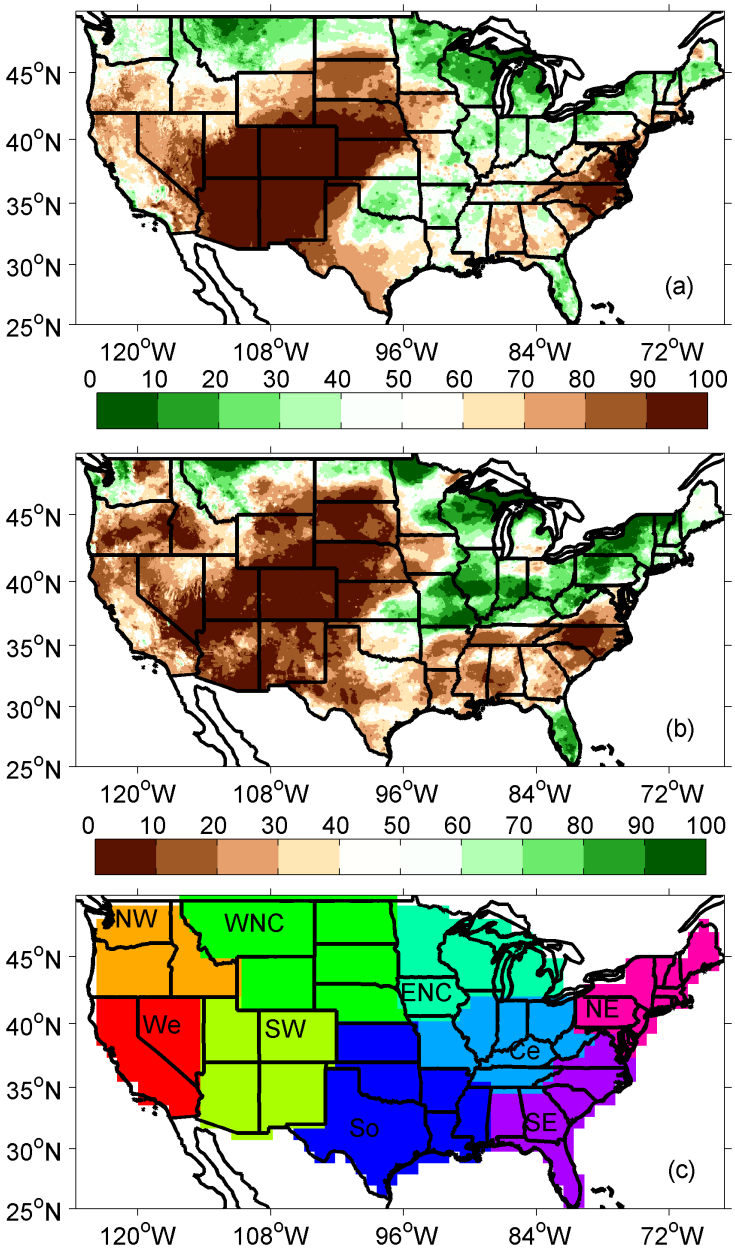

Figure 1: Accumulated ET_0 (a) and *Prcp* (b) anomaly percentiles from METDATA for AMJ 2002. Note that upper ET_0 and lower *Prcp* percentiles indicate drought (brown shading). NCDC climate regions (described in Section 2) on the CFSRF 1° grid used as area averaging domains for Section 3 results are shown in the bottom panel (c). Regions are named as follows: Northwest (NW), West (We), Southwest (SW), West North Central (WNC), South (So), East North Central (ENC), Central (Ce), Southeast (SE), and Northeast (NE).

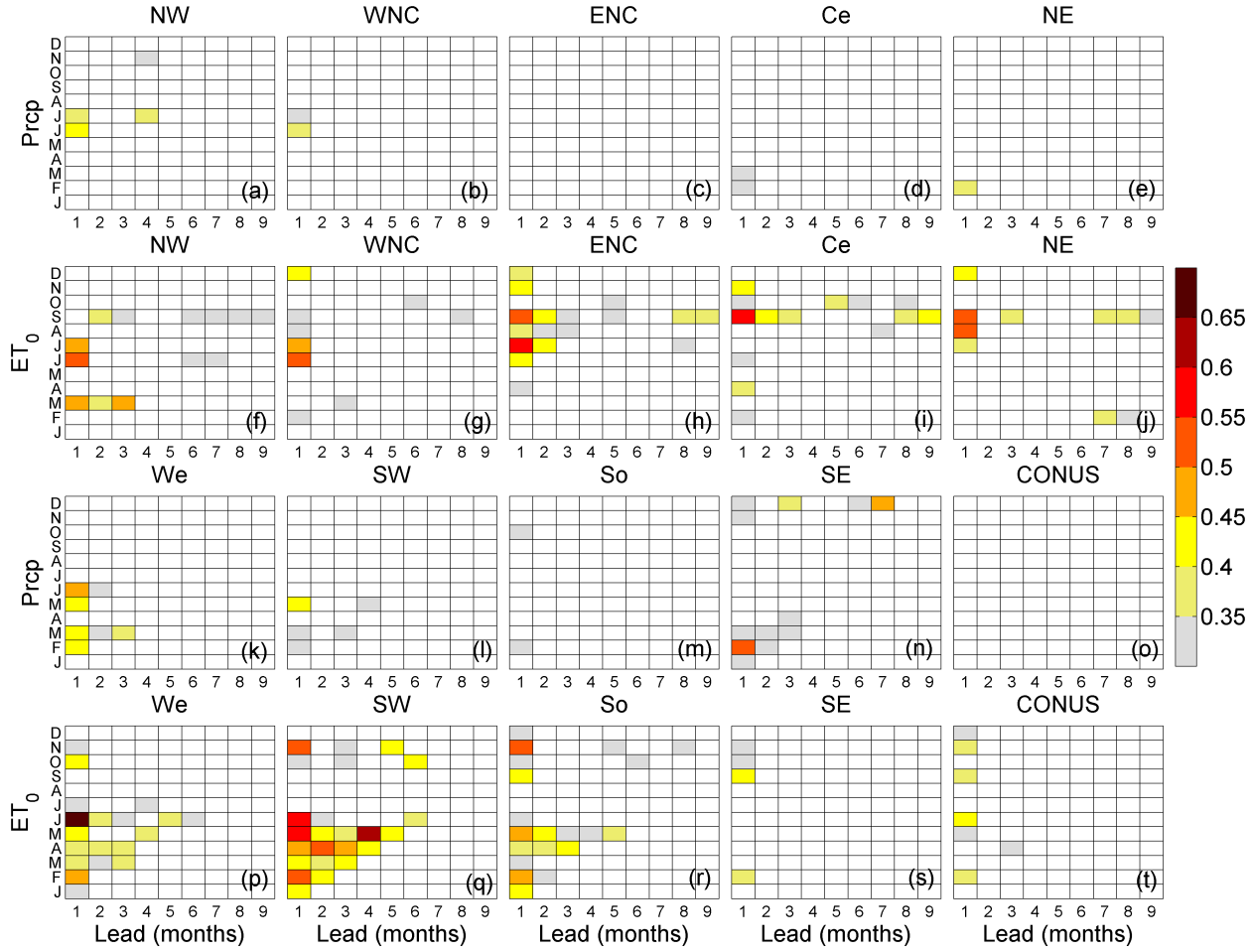

Figure 2. Average ET_0 (f-j and p-t) and *Prcp* (a-e and k-o) anomaly correlation (AC) between METDATA and CFSRF over each region (refer to Figure 1c for full region names and locations). Labels on the x-axis indicate lead time (months) and labels on the y-axis indicate the month for which the forecast is made. White boxes indicate AC < 0.3, which corresponds to p > 0.06 using a one-tailed probability.

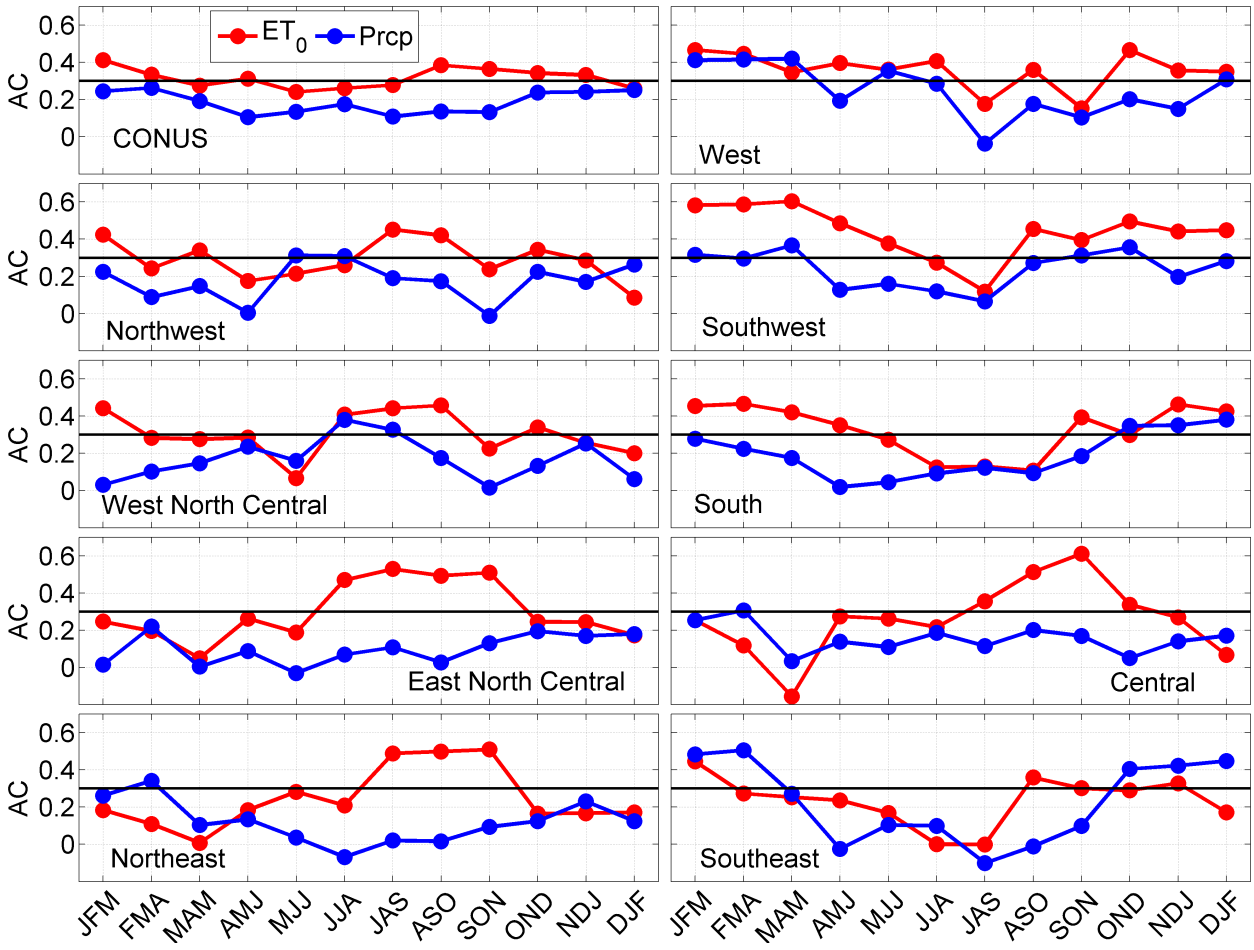

392

393 Figure 3. Season-one anomaly correlation area-averaged over CONUS and individual climate
394 regions. The black reference line indicates an anomaly correlation of 0.3, which represents the
395 start of moderate skill according to the CPC.

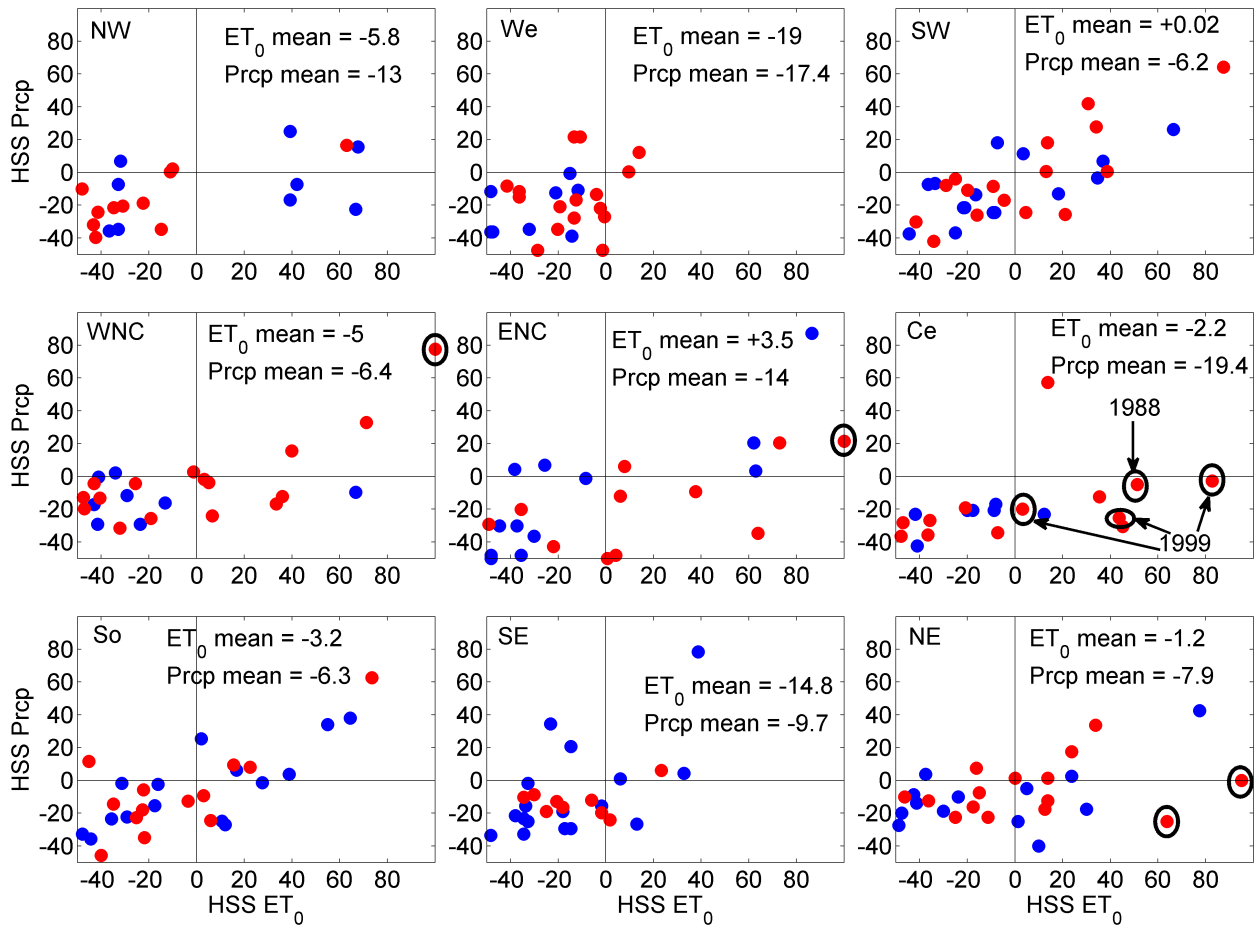

Figure 4. The HSS for season-one forecasts for cases when both ET_0 and *Prcp* indicate drought (>80th percentile for ET_0 and <20th percentile for *Prcp*). Labels inside of each panel indicate region and mean HSS. Black circles show notable drought events of JJA 1988 in the WNC, ENC, and Ce, JAS, ASO, and SON 1999 in the Ce, and MJJ and JJA 1999 in the NE. These events are described in detail in the text. Red dots are for warm seasons (AMJ, MJJ, JJA, JAS, ASO, and SON) and blue dots are for cold seasons (OND, NDJ, DJF, JFM, FMA, and MAM).

404

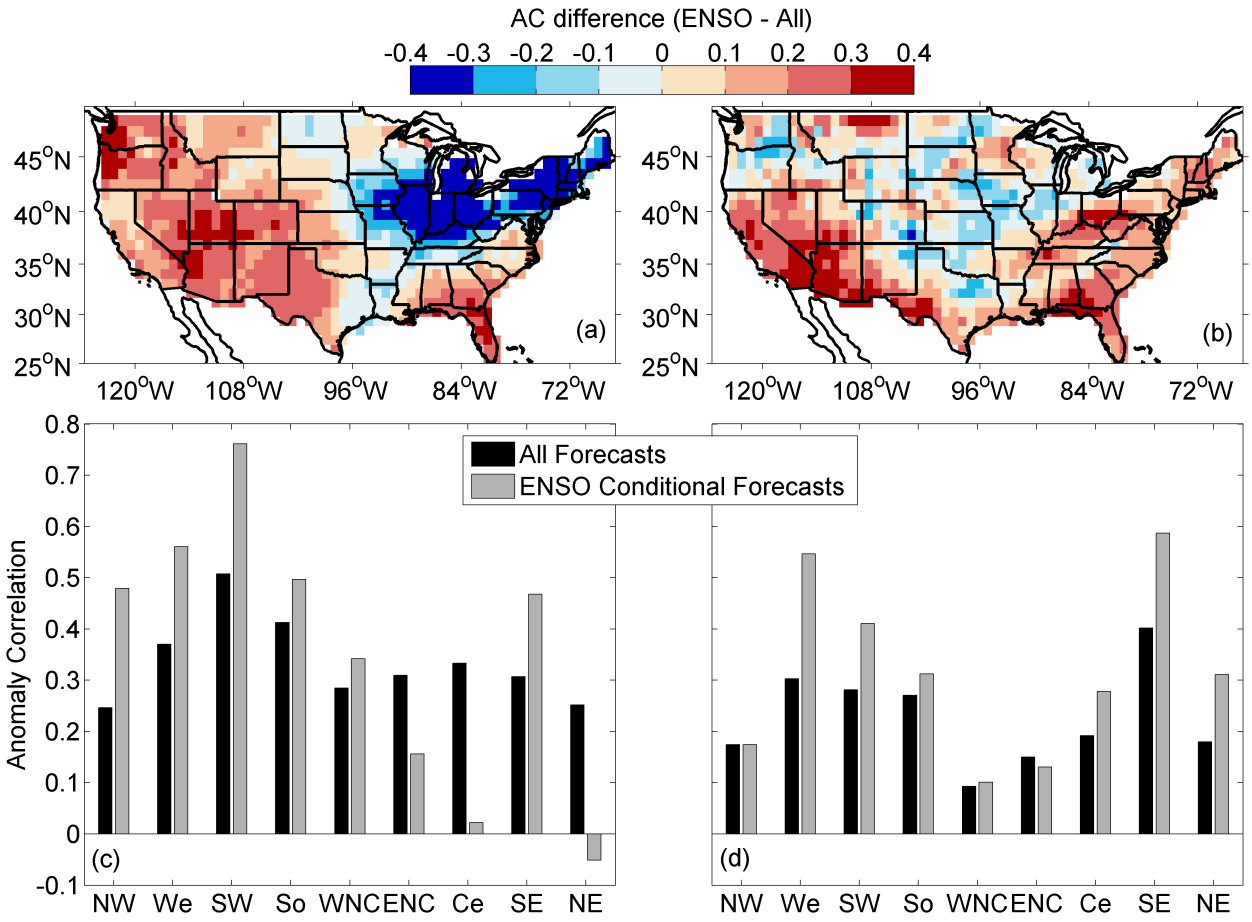

405
406

407 Figure 5. The difference in AC (fall-winter ENSO conditional forecasts minus all fall-winter
408 forecasts) and regionally averaged AC for ET_0 (a and c) and *Prcp* (b and d) forecasts.

Geophysical Research Letters

Supporting Information for

Improved Seasonal Drought Forecasts using Evaporative Demand Anomalies

Daniel J. McEvoy[1, 2], Justin L. Huntington[1, 2], John F. Mejia[1], and Michael T. Hobbins[3, 4]

[1]Desert Research Institute, Reno, Nevada, USA, [2]Western Regional Climate Center, Reno, Nevada, USA, [3]Cooperative Institute for Research in Environmental Sciences, Boulder, Colorado, USA, [4]NOAA Earth System Research Laboratory, Physical Sciences Division, Boulder, Colorado, USA

Contents of this file

Introduction

This supplement provides supporting information including:

- A brief discussion on the comparison of CONUS percent area in drought as depicted by reference evapotranspiration (ET_0) and precipitation (*Prcp*) anomalies to demonstrate a detailed look at the utility of ET_0 as a drought metric (Text S1).
- A figure demonstrating that ET_0 identifies similar drought events compared to *Prcp* over CONUS (Figure S1).
- Figures showing monthly skill of the individual drivers of ET_0 including maximum temperature, minimum temperature, specific humidity, downwelling shortwave radiation at the surface and wind speed (Figures S2 through S6).
- A table that provides details on initialization dates and number of members for each CFSv2 monthly ensemble (Table S1).
- Text describing the details of the Heidke Skill Score calculation procedure (Text S2).
- The equation to compute the Heidke Skill Score (Equation S1).

Text S1. Comparison of ET_0 and Prcp CONUS droughts

Figure S1 shows the CONUS average percent area in drought based on percentiles of three-month accumulated ET_0 (Figure S1 a) and *Prcp* (Figure S1 b), with drought being defined as ET_0 values above the 80th percentile and *Prcp* values below the 20th percentile. While differences in intensity and timing certainly exist, both metrics consistently identify the major drought periods of 1987-1989, 1999-2003, and 2006-2007. The wet periods of 1982-1984 (excluding summer of 1983) and 1991-1998 are also consistent. Much of CONUS experienced well above normal temperatures during 2006 and 2007, which likely drove the percent area of drought based on ET_0 much higher relative to non-uniform spatial distribution of *Prcp*.

Text S2. Heidke Skill Score details

In equation S1, *h* is the number of grid points with hits, or correct highest probability tercile forecasts, *t* is the total number of grid points, and *e* is the number of grid points expected to be correct by chance (i.e., *t*/3). All forecasts were used, including "equal chances". For the case of "equal chances", when there is exactly a 1/3 probability forecast for each tercile (above normal, near normal, and below normal), 0.333 is added to the h tally instead of 1. If a two-way tie occurs (1/2 probability forecast for two terciles) 0.5 is added to the *h* tally. Negative HSS indicates lower skill than the reference forecast (climatology), an HSS of zero indicates the same skill as the reference forecast, and positive HSS indicates skill as percent improvement over the reference forecast.

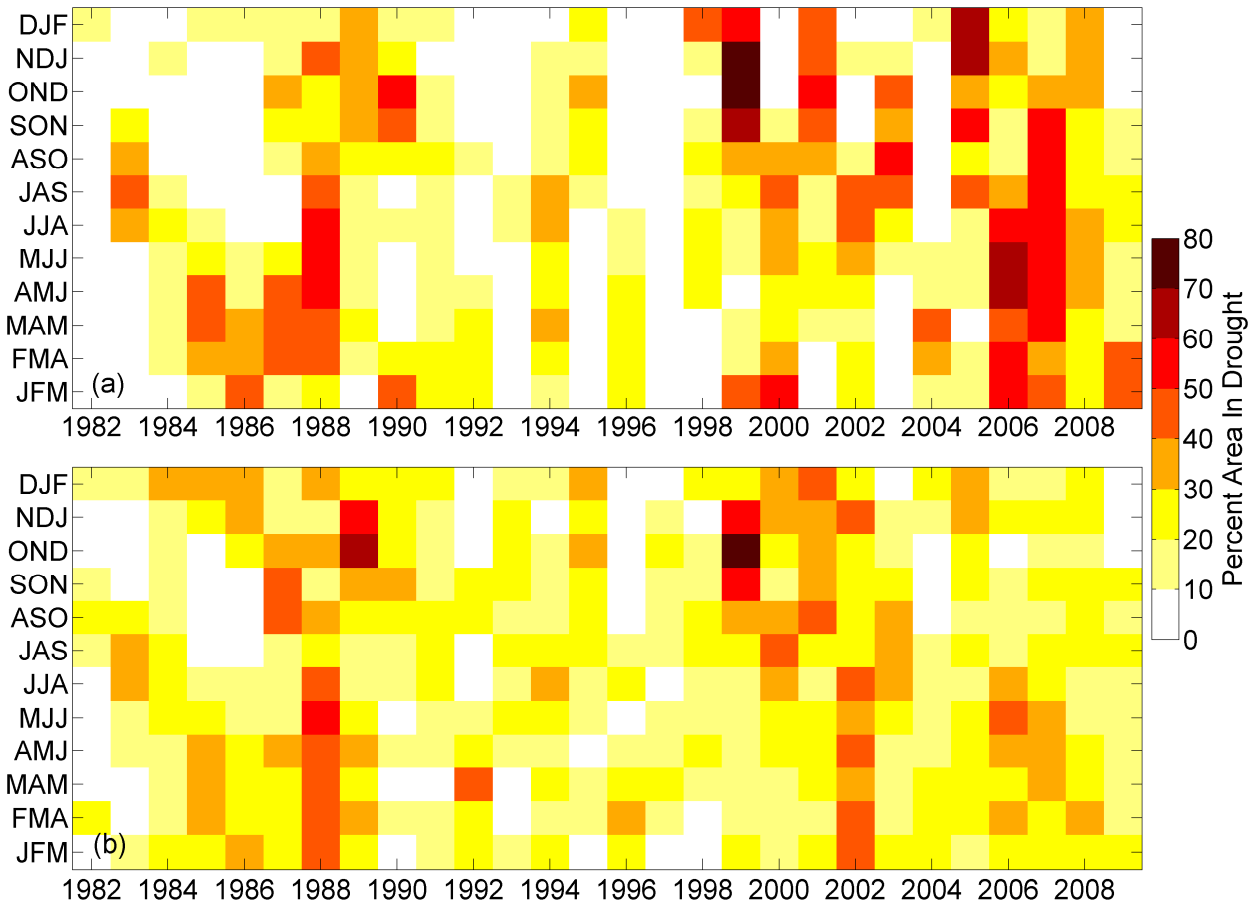

Figure S1. CONUS average percent area in drought based on three month accumulated ET0 (a) and Prcp (b) percentiles.

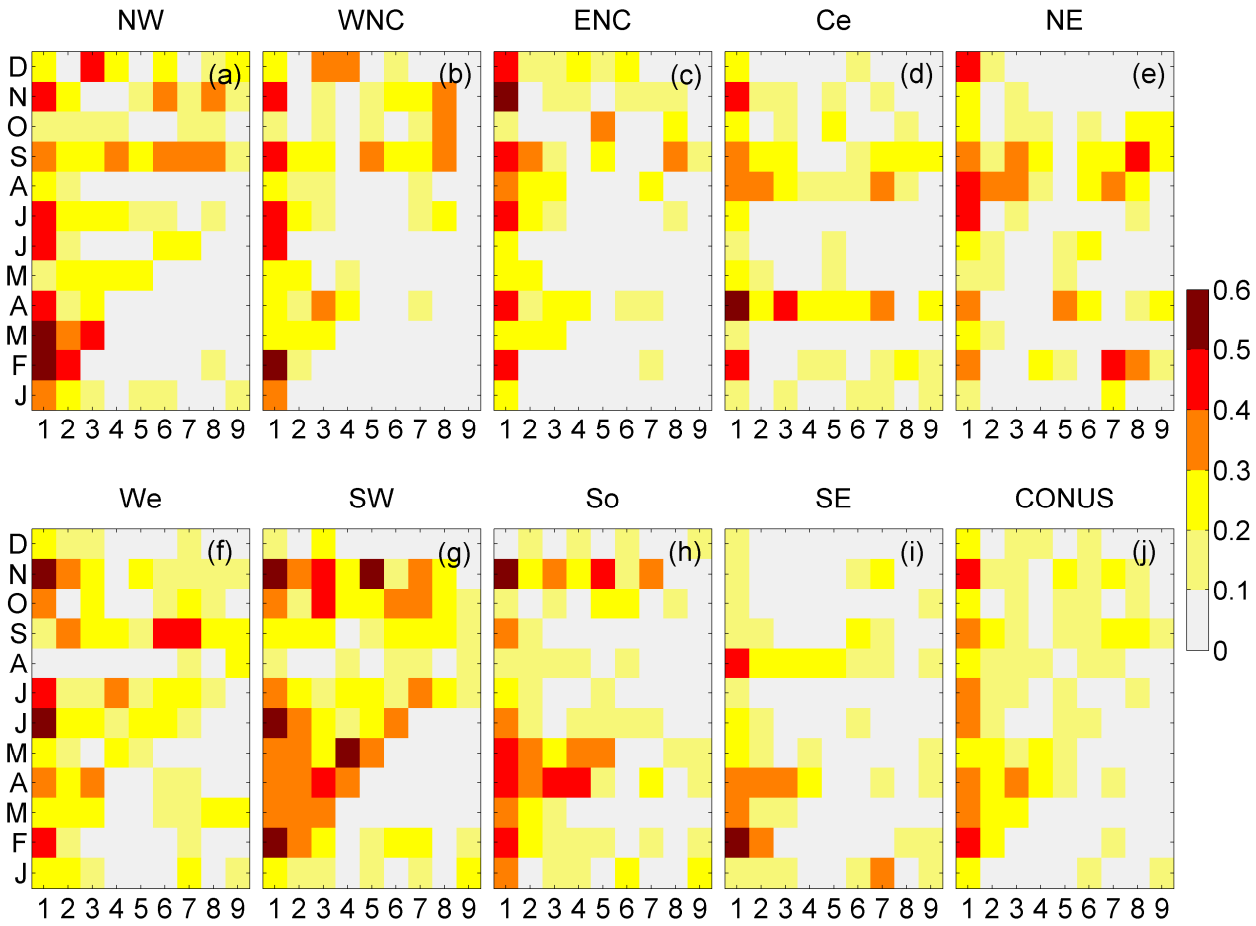

Figure S2. Average maximum temperature anomaly correlation between METDATA and CFSRF over each region (refer to Figure 1c in main manuscript for full region names and locations). Labels on the x-axis indicate lead time (months) and labels on the y-axis indicate the month for which the forecast is made.

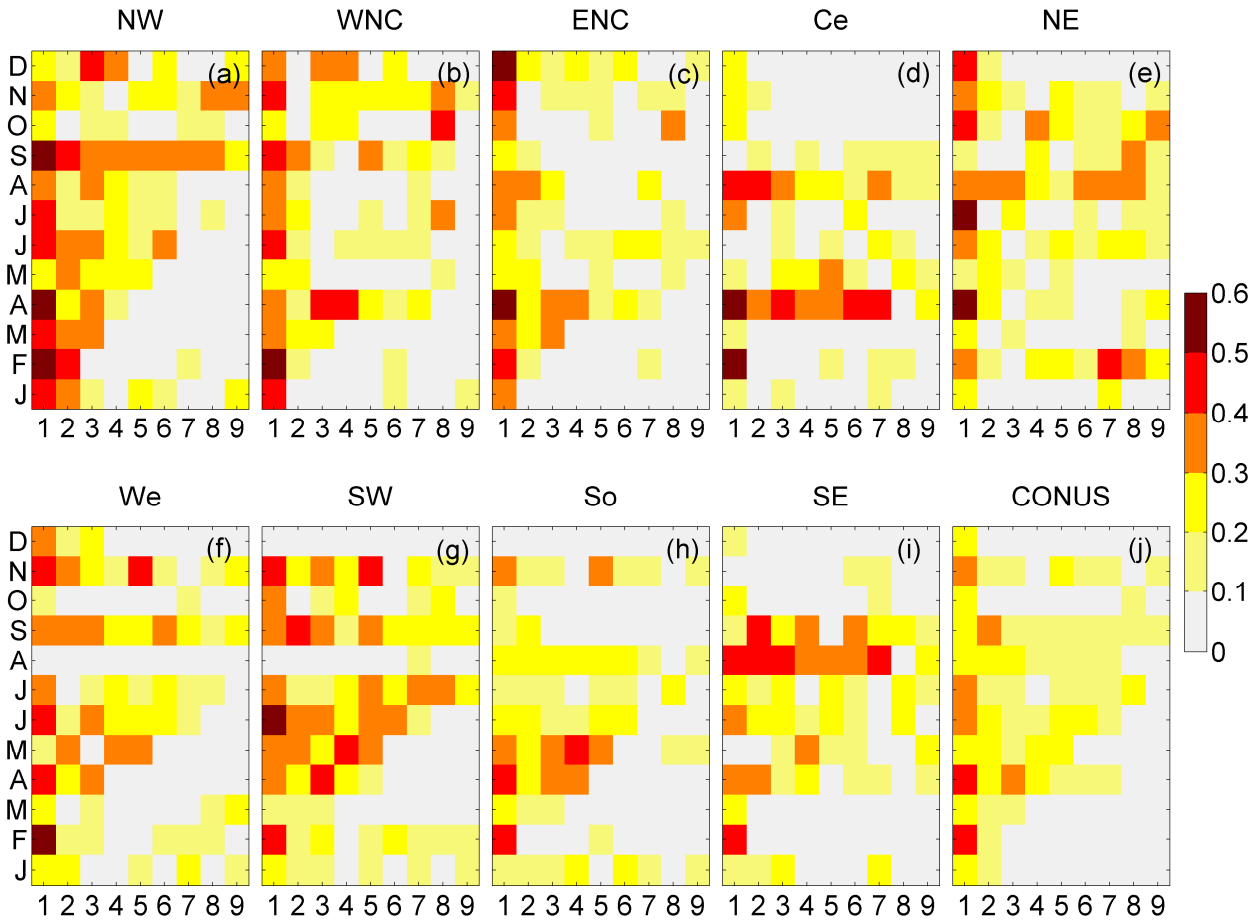

Figure S3. As in Figure S2, but for minimum temperature.

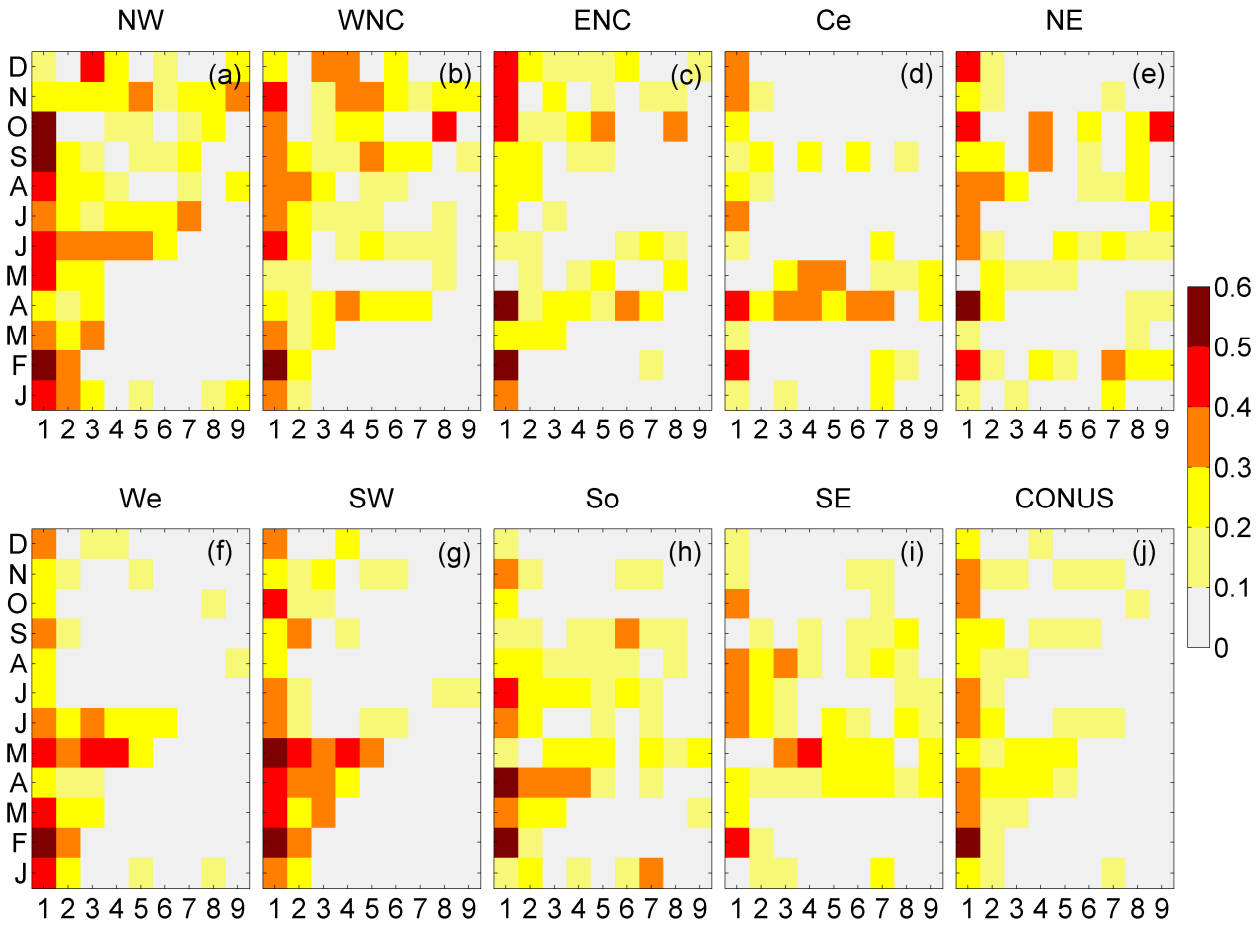

Figure S4. As in Figure S2, but for specific humidity.

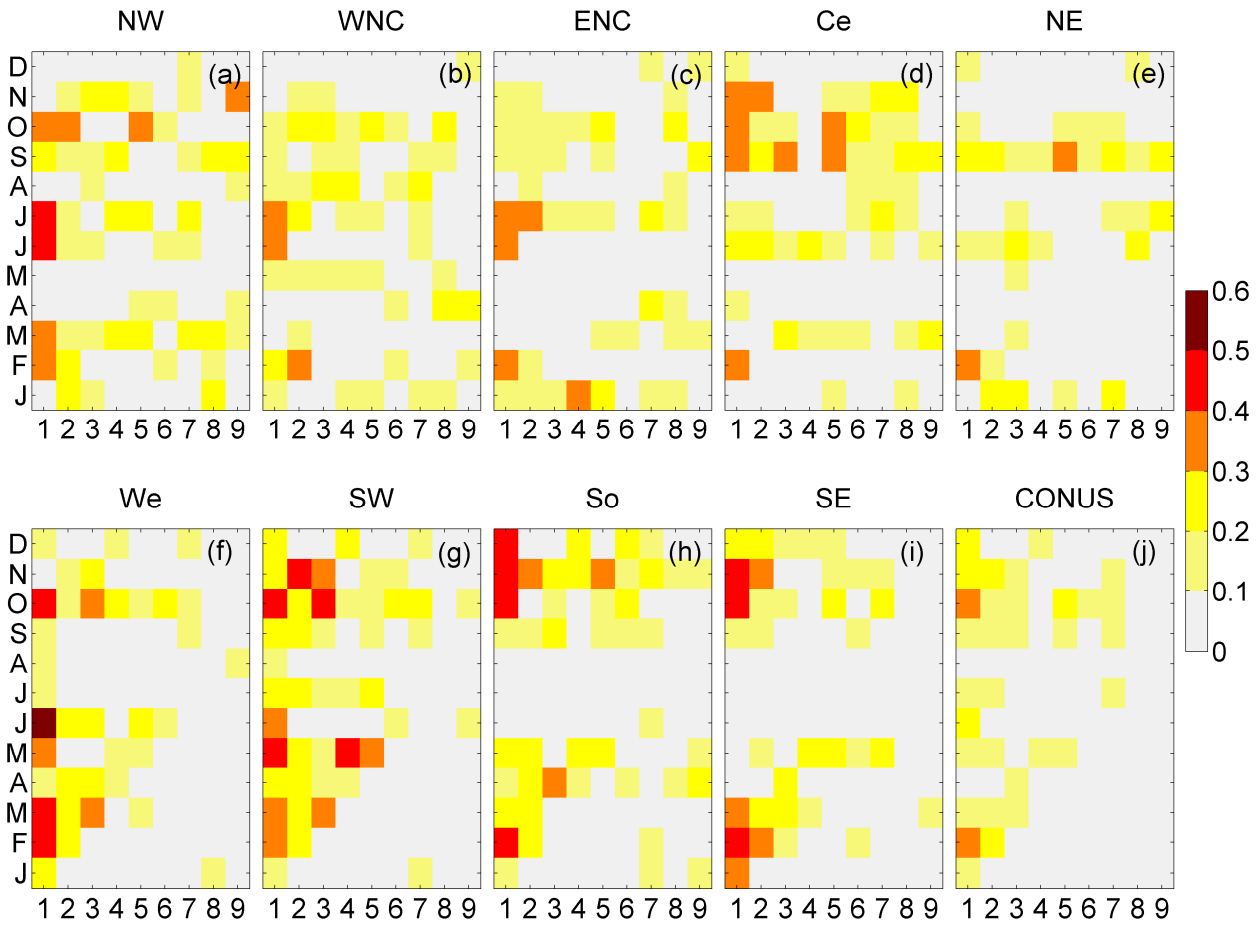

Figure S5. As in Figure S2, but for downwelling shortwave radiation at the surface.

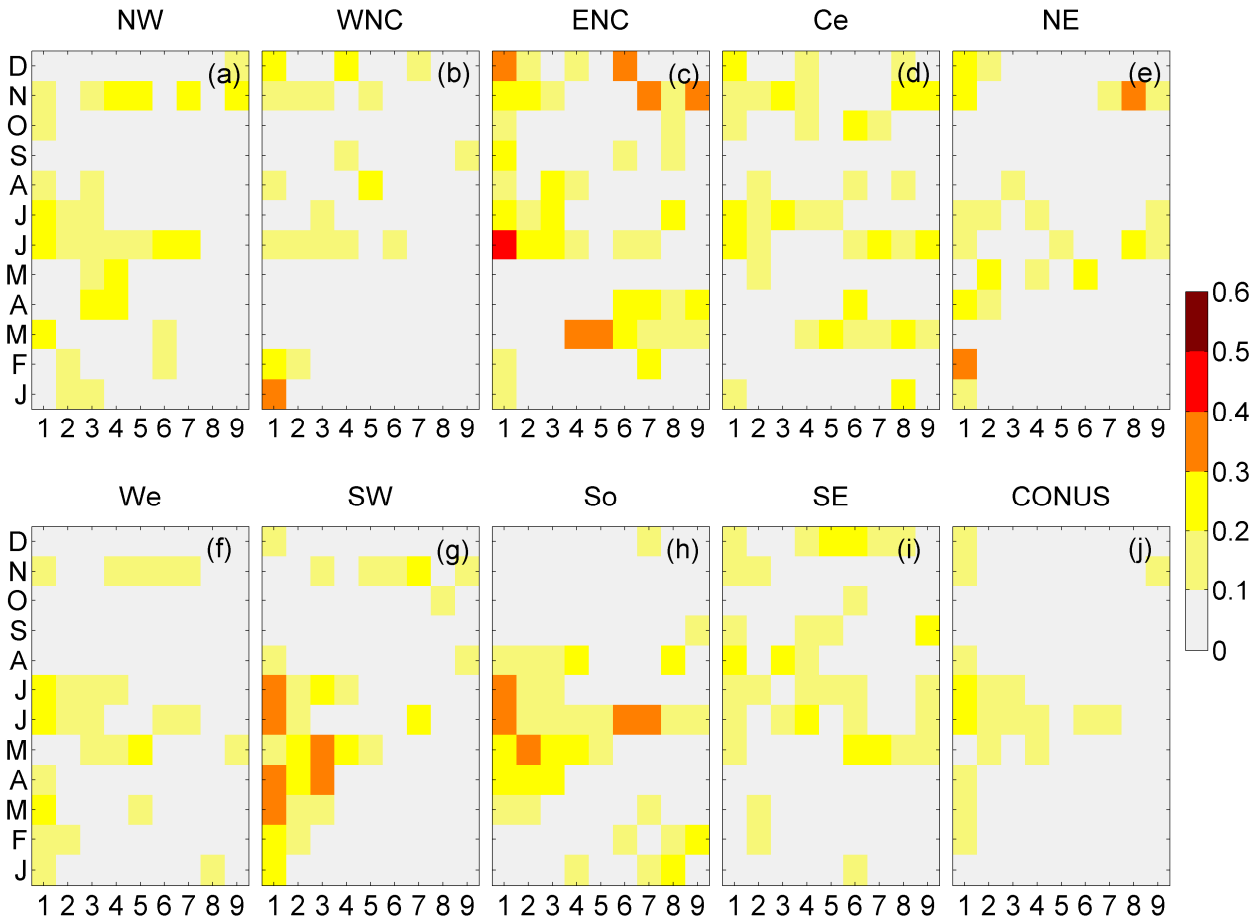

Figure S6. As in Figure S3, but for wind speed.

Initial Month	Number of Members	Initial Days
January	28	1, 6, 11, 16, 21, 26, 31
February	20	5, 10, 15, 20, 25
March	24	2, 7, 12, 17, 22, 27
April	24	1, 6, 11, 16, 21, 26
May	28	1, 6, 11, 16, 21, 26, 31
June	24	5, 10, 15, 20, 25, 30
July	24	5, 10, 15, 20, 25, 30
August	24	4, 9, 14, 19, 24, 29
September	24	3, 8, 13, 18, 23, 28
October	24	3, 8, 13, 18, 23, 28
November	24	2, 7, 12, 17, 22, 27
December	24	2, 7, 12, 17, 22, 27

Table S1. CFSv2 monthly ensembles are listed and each initial day consists of four members initialized at 00Z, 06Z, 12Z, and 18Z.

Equation S1:

$$HSS = \frac{(h - e) * 100}{(t - e)}$$